Spin-state transition in Ba_{2}Co_{9}O_{14}

J.-G. Cheng, J.-S. Zhou, Z. Hu, M. R. Suchomel, Y. Y. Chin, C. Y. Kuo, H.-J. Lin, J. M. Chen, D. W. Pi, C. T. Chen, T. Takami, L. H. Tjeng, and J. B. Goodenough

Phys. Rev. B **85**, 094424 — Published 23 March 2012

DOI: 10.1103/PhysRevB.85.094424

The spin-state transition in $Ba_2Co_9O_{14}$

J.-G. Cheng[1], J.-S. Zhou[1*], Z. Hu[2*], M. R. Suchomel[3], Y. Y. Chin[2], C. Y. Kuo[2], H.-J. Lin[4], J. M. Chen[4], D. W. Pi[4], C. T. Chen[4], T. Takami[5], L. H. Tjeng[2], and J. B. Goodenough[1]

[1] Materials Science and Engineering Program/Mechanical Engineering, University of Texas at Austin, Austin, TX 78712, USA

[2] Max Planck Institute for Chemical Physics of Solids, Nöthnitzerstr, 40, D-01187 Dresden, Germany

[3] Advanced Photon Source, Argonne National Laboratory, Argonne, Illinois 60439, USA

[4] National Synchrotron Radiation Research Center, HsinChu 30077, Taiwan

[5] Department of Physics, Graduate School of Science, Osaka University, 1-1 Machikaneyama-cho, Toyonaka, Osaka 560-0043, Japan

Abstract

$Ba_2Co_9O_{14}$ is a charge-ordered $Co^{2+/3+}$ cobaltite that consists of building blocks of CdI_2-type $Co^{2+/3+}O_{6/3}$ layers, face-shared $Co^{3+}{}_3O_{12}$ octahedral trimers, and corner-sharing $Co^{2+}O_4$ tetrahedra. The Co-$L_{2,3}$ XAS spectrum at room temperature indicates a high and a low spin state for Co^{2+} and Co^{3+} ions, respectively. Measurements of high-temperature resistivity and thermoelectric power revealed an insulator-to-insulator phase transition at T_t = 570 K, above which the inverse magnetic susceptibility $\chi^{-1}(T)$ deviates from the Curie-Weiss law. By using a combination of soft x-ray absorption spectroscopy at the O-K edge and high-resolution synchrotron x-ray powder diffraction measurements on crossing T_t, we have successfully determined the origin of this phase transition as a low-to-higher spin-state transition of Co^{3+} ions within the face-shared Co_3O_{12} octahedral trimers in $Ba_2Co_9O_{14}$.

I. Introduction

Layered cobalt oxides have attracted renewed interest in recent years owing to the observation of promising thermoelectric properties in Na_xCoO_2 [1] and of superconductivity in the bilayer hydrated $Na_{0.35}CoO_2 \cdot 1.3H_2O$.[2] The crystal structure of Na_xCoO_2 can be described as alternate stacking of CdI_2-type $CoO_{6/3}$ layers with randomly distributed Na layers. Extensive investigations have led to the identification of several misfit-layered cobaltites such as $[Ca_2CoO_3][CoO_2]_{1.62}$ [3] and $[Pb_{0.7}Sr_{1.9}Co_{0.4}O_3][CoO_2]_{1.8}$ [4]; they all have a similar mixed-valent CdI_2-type $Co^{3+/4+}O_{6/3}$ layer and exhibit a relatively high thermoelectric power and a low resistivity. In addition to charge and orbital degrees of freedom, the cobaltites containing Co^{3+} at octahedral sites also exhibit different spin states, *i.e.* a low spin (LS, $t_{2g}^6 e_g^0$, S = 0), a high spin (HS, $t_{2g}^4 e_g^2$, S = 2), and even an intermediate spin (IS, $t_{2g}^5 e_g^1$, S = 1) state.[5, 6] Spin-state transitions are generally believed to be associated with the unconventional transport properties of cobaltites [7] and the spin-blockade phenomena found in $RBaCo_2O_{5.5}$ [8, 9, 10, 11] and $La_{2-x}Sr_xCoO_4$ series [12].

Recently, Sun *et al.* [13] reported the synthesis and crystal structure of a barium cobaltite $Ba_2Co_9O_{14}$ that also contains CdI_2-type $CoO_{6/3}$ layers. However, it is an insulator below room temperature and orders antiferromagnetically below $T_N \approx 40$ K. The detailed magnetic structure of $Ba_2Co_9O_{14}$ was subsequently investigated by Ehora *et al.* [14] using neutron diffraction. Fig. 1 displays the crystal structure of $Ba_2Co_9O_{14}$, which can be described as an intergrowth of CdI_2-type $CoO_{6/3}$ layers and Co_3O_{12} octahedral trimers that are interconnected by corner-sharing CoO_4 tetrahedra. As shown in Fig. 1, there are five crystallographically independent Co sites in two types of coordination polyhedra: the Co2 octahedron shares its opposite triangular faces with two Co1 octahedra forming the Co_3O_{12} octahedral trimer; the Co4 and Co5 octahedra share edges to form the CdI_2-type layer with a 2:1 ordered arrangement within a 2D triangular lattice; Co3 tetrahedra share corners with both the Co_3O_{12} trimers and the CdI_2 layers. Co1, Co2 and Co4 ions are trivalent (Co^{3+}) and diamagnetic in a LS state, while Co3 and Co5 ions are divalent (Co^{2+}) with a HS configuration (S = 3/2). These HS Co^{2+} ions in the matrix of LS Co^{3+} ions are coupled through Co-O-O-Co "superexchange" interactions, which give rise to a

complex antiferromagentic ordering below $T_N \approx 40$ K.[14] Given that the LS Co^{3+} ions within the Co_3O_{12} octahedral trimers do not contribute to the electronic conduction, a charge ordering of the trivalent Co4 and divalent Co5 sites within the CdI_2 layers makes $Ba_2Co_9O_{14}$ an insulator, which is in contrast to the conductive mixed-valent $Co^{3+/4+}O_{6/3}$ layers in other layered cobaltites mentioned above.

Ehora *et al.* [11] have extended the resistivity measurement up to 900 K and observed a broad transition to another insulator phase with a smaller energy gap at $T > T_t \approx 600$ K. They have attributed this change to the creation of oxygen vacancies because their thermogravimetric data exhibited a small weight loss of 0.2 oxygen atoms per formula in the temperature range from room temperature to ~ 730 K. However, the phase with a wider energy gap was not recovered when the sample was reoxidized upon further heating above 730 K. This observation indicates that the anomaly of $\rho(T)$ at T_t may have little to do with the change of oxygen concentration. Alternatively, the insulator-insulator transition in $Ba_2Co_9O_{14}$ could be caused by (a) a thermally driven spin-state transition from LS Co^{3+} to higher-spin states at elevated temperatures like the well-known case of the perovskite $LaCoO_3$,[15] or (b) melting of the charge ordering on the Co4 and Co5 sites within the CdI_2-type layers.

In order to elucidate the origin of this transition, we have comprehensively characterized $Ba_2Co_9O_{14}$ above room temperature through measurements of resistivity, thermoelectric power, magnetic susceptibility, and soft x-ray absorption spectroscopy at the Co-$L_{2,3}$ and O-K edge, and high-resolution synchrotron x-ray powder diffraction. Our high-temperature resistivity data is nearly identical to that obtained by Ehora *et al.*[14], which confirms an insulator-insulator transition in our $Ba_2Co_9O_{14}$ sample. However, instead of their proposed electron doping model induced by oxygen deficiency created near T_t, our high-temperature spectroscopy and structural studies support a scenario in which the insulator to insulator transition is due to a low-to-higher spin-state transition of the Co^{3+} ions within the face-shared octahedral trimers.

II. Experimental Details

Polycrystalline $Ba_2Co_9O_{14}$ samples were prepared through a conventional solid-state reaction from a stoichiometric mixture of $BaCO_3$ and Co_3O_4 in air. Details about sample synthesis and characterizations of the physical properties below room temperature can be found elsewhere [16]. The high-temperature resistivity and thermoelectric power were measured simultaneously with a homemade device in the temperature range $300 < T < 773$ K in an Ar atmosphere. Magnetic-susceptibility measurements were carried out in a vacuum of 10^{-3} torr with a commercial Superconducting Quantum Interference Device (SQUID) magnetometer (Quantum Design) from 300 to 750 K. These measurements have been performed during heating up and cooling down. The soft X-ray absorption spectroscopy (XAS) at the Co-$L_{2,3}$ and O-K edges on the polycrystalline $Ba_2Co_9O_{14}$ samples were measured at the BL11A and BL08B beam lines of the National Synchrotron Radiation Research Center (NSRRC) in Taiwan. The Co-$L_{2,3}$ and O-K XAS spectra were taken in the total-electron-yield (TEY) mode and the fluorescence yield (FY) mode with a photon energy resolution of 0.3 eV and 0.2 eV, respectively. Clean sample surfaces were obtained by cutting pellets *in situ* just before collecting the data in an ultrahigh vacuum chamber with a pressure in the low 10^{-9} mbar range. High-resolution synchrotron X-ray powder diffraction (SXRD) data were collected upon heating from 298 to 872 K on beamline 11-BM (λ = 0.41219 Å) at the Advanced Photon Source, Argonne National Laboratory [17]. The obtained SXRD patterns were analyzed by the Rietveld method with the FULLPROF program[18].

III. Results and Discussion

Fig. 2 displays the temperature dependences of resistivity $\rho(T)$ and thermoelectric power $S(T)$ of the $Ba_2Co_9O_{14}$ sample measured on cycling between 300 and 773 K in an Ar atmosphere. In accordance with the report by Ehora *et al.*[11], our $\rho(T)$ data confirm a broad insulator-insulator transition at T_t. We have defined T_t = 570 K as the peak temperature in the plot of $d\ln\rho/d(1/T)$ *vs*. $1/T$, inset of Fig. 2. The $\rho(T)$ data measured during heating up and cooling down overlap each other. The $S(T)$ curve also shows an anomaly near T_t. $S(T)$ is nearly temperature independent at $T < 530$ K, which is typical for a polaronic conductor. Given the insulator-insulator transition deduced from the $\rho(T)$

measurement, a sharp decrease of S at $T > T_t$ indicates that the transition is associated with releasing mobile charge carriers at $T = T_t$. Although the S(T) data measured during cooling down overlaps that on heating up at high temperatures, the sample shows a lower S at $T < T_t$ after one thermal cycle. It is clear that the oxygen concentration for this p-type conductor is slightly reduced during the high-temperature measurement. However, the abrupt mobile charge carrier release near T_t should be distinguished from the gradual charge carrier increase taking place at high temperatures.

Fig. 3 displays the paramagnetic susceptibility $\chi(T)$ and its inverse $\chi^{-1}(T)$ upon thermal cycling between 300 and 750 K under an external magnetic field H = 2 T. $\chi^{-1}(T)$ shows a nearly linear behavior and no difference for measurements during heating up and cooling down below 570 K. The slight reduction of oxygen concentration as seen from the high-temperature S(T) measurement in Fig. 2 does not alter the magnetic properties below T_t. From the Curie-Weiss (C-W) fitting we obtained an effective paramagnetic moment μ_{eff} = 7.36 μ_B/f.u. and a Weiss temperature θ = 44.8 K within $300 < T < 570$ K. In accordance with the long-range antiferromagentic ordering at $T_N \approx 40$ K, a negative $\theta = -50.9$ K has been obtained by Ehora *et al.* [14] from a C-W fitting to $\chi^{-1}(T)$ below 300 K. But a closer inspection of the $\chi^{-1}(T)$ data in Ref. 11 revealed that the slope of $\chi^{-1}(T)$ increases gradually with temperature, which is consistent with a positive θ that we have obtained within the temperature range $300 < T < 570$ K. A temperature-dependent Weiss constant may reflect a contribution from unquenched orbital angular momentum, which makes the C-W law invalid in some cases.[19] Ehora *et al.*[14] have found that the μ_{eff} from $\chi(T)$ below room temperature is significantly larger than the expected spin-only value of 5.74 μ_B/f.u. for a S = 3/2 state on HS Co3 and Co5 sites, which supports an orbital contribution and/or some thermal excitations to a higher spin state. For $T > 570$ K, $\chi^{-1}(T)$ deviates obviously from C-W behavior and a hysteresis loop develops in the temperature range $660 < T < 750$ K. This observation might indicate that some of the LS Co^{3+} ions at Co1, Co2, and/or Co4 sites are transforming to a higher spin state above 570 K.

To probe directly the valence and spin states of the Co ions in $Ba_2Co_9O_{14}$, we turn to the more sensitive XAS measurements at the Co-$L_{2,3}$ and O-K absorption edges. The Co ($2p \rightarrow 3d$) transitions at the Co-$L_{2,3}$ edge involve directly the relevant valence shell and are extremely sensitive to the charge and spin states. The profile of an XAS spectrum reveals information about the valence and spin states [9, 20, 21, 22, 23]. First, we have checked the valence state and the spin states of Co ions at room temperature by using the Co-$L_{2,3}$ XAS spectrum. Fig. 4 displays the room-temperature Co-$L_{2,3}$ XAS spectrum of $Ba_2Co_9O_{14}$ together with that of Sr_2CoO_3Cl [18], $LiCoO_2$ [24], $YBaCo_3AlO_7$ [25] and CoO that serve as the references for the HS-Co^{3+}, the LS-Co^{3+}, the tetrahedral-site HS-Co^{2+}, and the octahedral-site HS-Co^{2+}, respectively. We have removed the Ba $M_{4,5}$ white lines located at 784 and 798 eV by using the Ba $M_{4,5}$ spectrum of $YBaZn_3AlO_7$. The Co spectra of the different valence and spin configurations show quite different multiplet structures. One can see that the Co^{2+} spectra of CoO and $YBaCo_3AlO_7$ contain peaks that are located at least 2 eV below the main peak of the Co^{3+} spectra. While the main peaks for both Co^{2+} lie at around 779 eV, the main peaks for both Co^{3+} lie at 780.5 eV. This is consistent with the generally accepted notion that an increase of the valence state from Co^{2+} to Co^{3+}, for example, typically results in a shift of the $L_{2,3}$ XAS spectra to higher energies by 1 eV or more.[9, 22] We note that the lowest energy peak at 777.8 eV is characteristic of an octahedral-site Co^{2+}. Compared to the HS Sr_2CoO_3Cl, the LS $LiCoO_2$ has a higher intensity at the L_2 edge with a rather sharp peak at 795 eV. As for the $Ba_2Co_9O_{14}$ spectrum, the profile can be decomposed into at least two components, one at 777.8 eV and 779 eV which is close to Co^{2+} in the reference compound CoO and another at 795 eV for the Co-L_2 edge from LS Co^{3+}. These observations strongly suggest the presence of Co^{2+} and LS Co^{3+} ions in this material, which is highly consistent with results from previous NPD refinements.[14] To further verify this hypothesis, we carried out a simulation by adding spectra from the as-measured CoO, $YBaCo_3AlO_7$ and $LiCoO_2$ with a ratio of 2/9 Co^{2+}(Tet.) + 1/9 Co^{2+} (Oct.) + 6/9 Co^{3+} (Oct.) and compared the result of $Ba_2Co_9O_{14}$. As seen in Fig. 4, the match between the experimental spectrum and the simulated one is nearly perfect. In contrast, the simulated spectrum is quite different from that of $Ba_2Co_9O_{14}$, if the spectrum from $LiCoO_2$ is replaced by that of Sr_2CoO_3Cl; the

difference becomes more prominent at the L_2 edge. Therefore, the Co-$L_{2,3}$ XAS results establish that that all Co^{3+} ions in $Ba_2Co_9O_{14}$ are in the LS state at room temperature.

After clarifying the valence and spin states on the cobalt sites at room temperature, we now investigate the possibility of a spin-state transition as the temperature increases by using the O-K XAS spectrum, which was measured with a bulk-sensitive fluorescence-yield (FY) method. The advantage of FY O-K XAS spectrum is to minimize the signal from the sample surface where some of the oxygen might be lost to the vacuum at high temperatures. Fig. 5 displays the temperature dependent O-K XAS spectra of $Ba_2Co_9O_{14}$. Here, we are mainly interested in the lowest lying states, *i.e.*, the unoccupied states related to the Co^{3+} ions [9, 18, 26]. These states are located at the pre-edge region below 532 eV and originated from transitions from the O 1s core level to the O 2p orbitals that are mixed into the unoccupied Co 3d states [9, 18, 19, 23]. For a LS Co^{3+} below 300 K with the $t_{2g}^6 e_g^0$ configuration, the lowest energy structure in the O-K spectrum at about 530.5 eV is due to the transitions from the O1s core level into the unoccupied Co 3d e_g states since the low lying t_{2g} orbitals are fully occupied. However, as the temperature increases to above room temperature, a lower energy spectral feature around 528.7 eV appears and becomes very pronounced above 510 K, whereas the peak at 530.5 eV loses its spectral weight. These temperature-dependent spectral changes are due to a spin-state transition of Co^{3+}, similar to that observed in $LaCoO_3$,[23] and reflect the fact that transitions to the lower lying t_{2g} orbitals are now allowed, *i.e.* the t_{2g} states are no longer fully occupied. In other words, at T > 300 K, some of the LS Co^{3+} ions in $Ba_2Co_9O_{14}$ transform into the HS $t_{2g}^4 e_g^2$ or IS $t_{2g}^5 e_g^1$ state.

In order to have a quantitative description of the temperature-dependent spectral weight transfer, we present in Fig. 6 the temperature dependent ISD from the O-K XAS, where ISD is the integration of signal $|I(T)-I(80K)|^2$, in which I(80K) and I(T) refer to the spectral intensity from 526.6 to 532.6 eV at 80 K and the temperatures above 80 K, respectively. From Fig. 6, we can see a dramatic increase of the ISD signal at T > 550 K reflecting an accelerated spin-state transition of Co^{3+}, in agreement with the observed anomalies in transport and magnetic properties in Figs. 1 and 2. In comparison with

$LaCoO_3$, the spectral weight transfer from an e_g- to a t_{2g}-related peak in the interval 80 < T < 630 K in the $Ba_2Co_9O_{14}$ spectra is weaker, indicating that there are fewer Co^{3+} ions contributing to the spin-state transition than in the $LaCoO_3$. Which of the Co^{3+} sites undergo the spin-state transition will now be addressed by the high-temperature structural study shown in the next section.

Since the spin-state transition of Co ions is always accompanied by a bond-length change,[27,28] a high-temperature structural study is critical to clarify this uncertainty. Moreover, the structural study also helps us to check the possibility of charge-order melting within the CdI_2-type layer. We therefore carried out a high-temperature synchrotron X-ray diffraction (SXRD) on $Ba_2Co_9O_{14}$ from 298 to 872 K over a broad range of the D space. Fig. 7 displays the SXRD patterns between $5 < 2\theta < 15°$. As can be seen, no symmetry change can be discerned on crossing T_t. The detailed structural evolution as a function of temperature has been extracted by using Rietveld refinements on these SXRD patterns with a structural model[11] defined in the space group *R-3m* (No. 166), with the Ba atom at 6c (*1/3, 2/3, z*), five Co atoms at 6c (*0, 0, z*), 3b (*0, 0, 1/2*), 6c (*2/3, 1/3, z*), 9e (*5/6, 1/6, 2/3*), and 3a (*1/3, 2/3, 2/3*) sites, and three oxygen atoms located at 18h (*x, y, z*) and 6c (*0,0,z*) positions. All refinements converged fairly well with typical reliability factors: $R_p \approx 10\%$, $R_{wp} \approx 12\%$ and $\chi^2 \approx 5.0\%$; the results are generally consistent with those obtained with both single-crystal diffraction (SCD)[10] and neutron powder diffraction (NPD)[11]. The structural parameters at 298 K are listed in Table I, including the unit-cell parameters, average <Co-O> bond lengths, and the calculated bond valence sum (BVS) for Co ions; the formula of BVS is given in the caption of Table I. The corresponding data from SCD [13] and NPD [14] are also included in Table I for comparison. The SXRD gives rise to high precision of D space and therefore results in one more decimal in the lattice parameters in comparison with those obtained from the SCD and the NPD. However, diffractions with a wavelength $\lambda = 0.41219$ Å carry less information about the oxygen positions, especially the oxygen around Co^{3+}, than that in the SCD and the NPD since the scattering to X-ray is sensitive to the total number of electrons. The less accurate Co-O bond lengths from SXRD leads to relatively small BVS in Table I.

Temperature dependences of the unit-cell parameters and the average <Co-O> bond lengths ($d_{Co\text{-}O}$) for all Co sites are shown in Figs. 8 and 9, respectively. Several important structural features can be clearly observed in the vicinity of T_t, which is marked by dotted lines: (1) a reflection point at T_t can be seen in all curves of *a*, *c* and *V* versus T; (2) whereas the bond lengths of $d_{Co4\text{-}O}$, and $d_{Co5\text{-}O}$ show no change or a slight decrease, $d_{Co1\text{-}O}$ and $d_{Co2\text{-}O}$ in the octahedral trimer expand dramatically in the vicinity of T_t = 570K. The temperature dependence of the average $d_{Co\text{-}O}$ for Co1 and Co2 from 300 to 800 K is not only out of the possible range of the thermal expansion in a typical perovskite oxide,[25] but also significantly higher than the bond-length change caused by the thermally driven LS to higher-spin transition in $LaCoO_3$ [24] in which the transition remains incomplete for temperatures up to 1000 K

The nearly temperature-independent $d_{Co4\text{-}O}$ indicates that the trivalent Co4 ion does not contribute to the spin-state transition. On the other hand, the dramatic change of $d_{Co1\text{-}O}$ and $d_{Co2\text{-}O}$ on crossing T_t confirmed that it is the trivalent Co1 and Co2 ions within the octahedral trimer that are responsible for the spin-state transition. The expansion of the Co_3O_{12} octahedral trimer due to the thermally driven spin-state transition also compresses the $Co3O_4$ tetrahedra that are connected via corner-shared O1 to Co_3O_{12} trimer, leading to a concomitant shrinkage of the average $d_{Co3\text{-}O}$ distance. The possibility of a charge-order melting at T_t within the CdI_2-type layers can be readily excluded because the Co 4 and Co 5 ions can be well-distinguished by the large difference between their $d_{Co\text{-}O}$ values in Fig. 9. However, the last few points of the $d_{Co4\text{-}O}$ at T > 830 K increase sharply, which may signal that the charge-ordering state within the CdI_2 layers of $Ba_2Co_9O_{14}$ is close to collapse.

IV. Conclusion

The cobaltite $Ba_2Co_9O_{14}$ undergoes an insulator-insulator transition spreading over a broad range of temperature around T_t = 570 K. The paramagnetic susceptibility deviates from a Curie-Weiss law as T_t is approached from low temperatures. The thermoelectric power S indicates that $Ba_2Co_9O_{14}$ is a p-type polaronic conductor at $T < T_t$; an abrupt

drop of S as temperature increases on crossing T_t indicates release of more mobile charge carriers. There are five Co sites occupied by Co^{2+} and Co^{3+} in the crystal structure of $Ba_2Co_9O_{14}$. The Co-$L_{2,3}$ XAS spectrum reveals that the Co^{3+} ions have the LS state below 300 K. By using bulk sensitive FY O-K XAS spectra, we show that a spin-state transition from the LS to a higher-spin state on Co^{3+} occurs at T_t. Structural details obtained from Rietveld analysis of high-temperature synchrotron powder X-ray diffraction data help us to identify the specific Co^{3+} sites of Co1 and Co2 where the spin-state transition takes place. Moreover, we find that the overall bond length change at these Co sites on crossing the spin-state transition is larger than the averaged Co^{3+}-O bond length change associated with the LS to higher spin transition found in $LaCoO_3$. Since the thermally driven spin-state transition in $LaCoO_3$ is incomplete at T < 1000 K, the saturation value of 2.05 Å found for averaged Co1-O and Co2-O bond length in $Ba_2Co_9O_{14}$ could be used as a reference for HS Co^{3+} at octahedral-sites. Finally, results from this structural study rule out the possibility of a collapse at T_t of the charge-ordered state in the CdI_2 structural layer containing Co4 and Co5 sites.

Acknowledgements

This work was supported by NSF (DMR 0904282, DMR 1122603, CBET 1048767) and the Robert A Welch foundation (Grant F-1066). Use of the Advanced Photon Source at Argonne National Laboratory was supported by the U. S. Department of Energy, Office of Science, Office of Basic Energy Sciences, under Contract No. DE-AC02-06CH11357.

jszhou@mail.utexas.edu
zhiwei.Hu@cpfs.mpg.de

Table I Comparison of the unit-cell parameters, average ⟨ Co-O ⟩ bond lengths, and the bond valence sum (BVS) of Co ions at 298 K obtained in the present and the previous studies. The Bond Valence Sum (BVS) model provides a phenomenological relationship between the formal valence of a bond and the corresponding bond lengths.[29,30] The valence S is the sum of the individual bond valences (s_i) for the Co-O bonds:

$BVS = \sum_i s_i = \sum_i \exp[(r_0 - r_i)/B_0]$, where $B_0 = 0.37$, $r_0 = 1.692$ for the Co^{2+}-O pair and r_0 = 1.637 for the Co^{3+}-O pair, respectively.

T = 298 K		This work (SXRD)	Ref. 13 (SCD)	Ref. 14 (NPD)
a (Å)		5.69464(3)	5.6958(4)	5.6963(8)
c (Å)		28.9017(2)	28.909(4)	28.924(6)
Co1 Oct.(Co^{3+},LS)	<Co-O>	1.944(2)	1.937	1.935
	BVS	2.62(2)	3.00	3.18
Co2 Oct.(Co^{3+},LS)	<Co-O>	1.962(3)	1.954	1.945
	BVS	2.49(2)	2.86	3.09
Co3 Tetr.(Co^{2+})	<Co-O>	1.913(4)	1.922	1.931
	BVS	2.20(2)	2.15	2.10
Co4 Oct.(Co^{3+},LS)	<Co-O>	1.933(1)	1.919	1.915
	BVS	2.73(1)	3.15	3.36
Co5 Oct.(Co^{2+},HS)	<Co-O>	2.082(1)	2.076	2.082
	BVS	2.089(6)	2.12	2.09

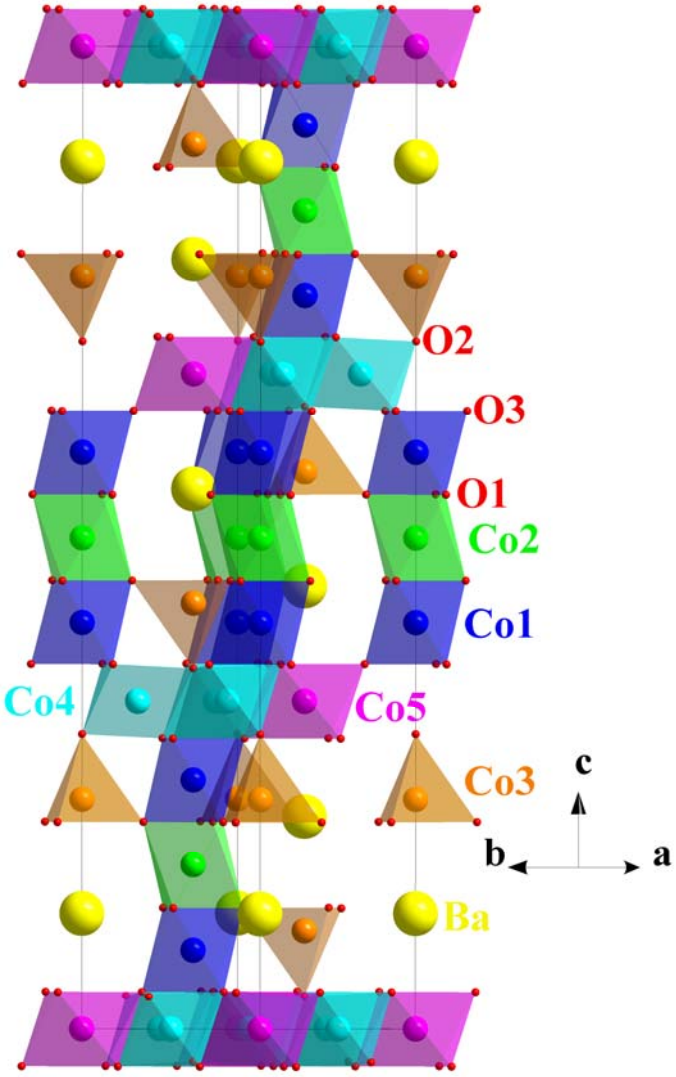

Fig. 1 (Color Online) Crystal structure of $Ba_2Co_9O_{14}$. Polyhedra colors distinguish the five crystallographically independent Co sites in the structure.

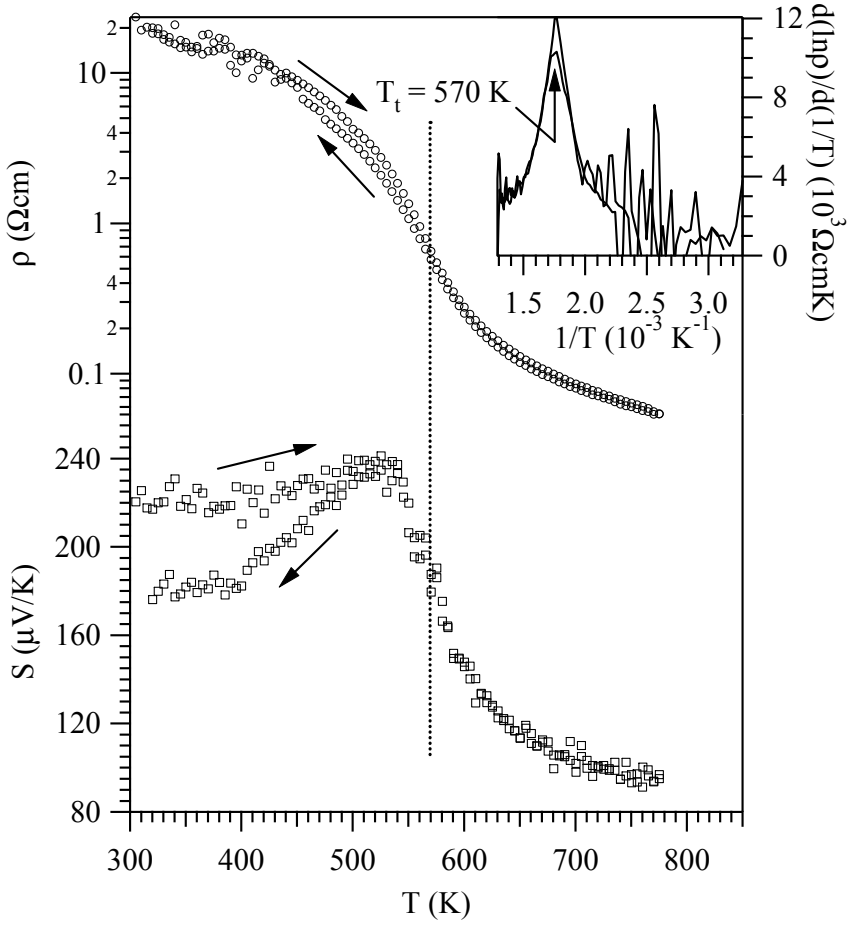

Fig. 2 Temperature dependences of resistivity ρ(T) and thermoelectric power S(T) measured on thermal cycling between 300 and 773 K. Transition temperature T_t = 570 K was determined from the peak of d(lnρ)/d(1/T) shown in the inset.

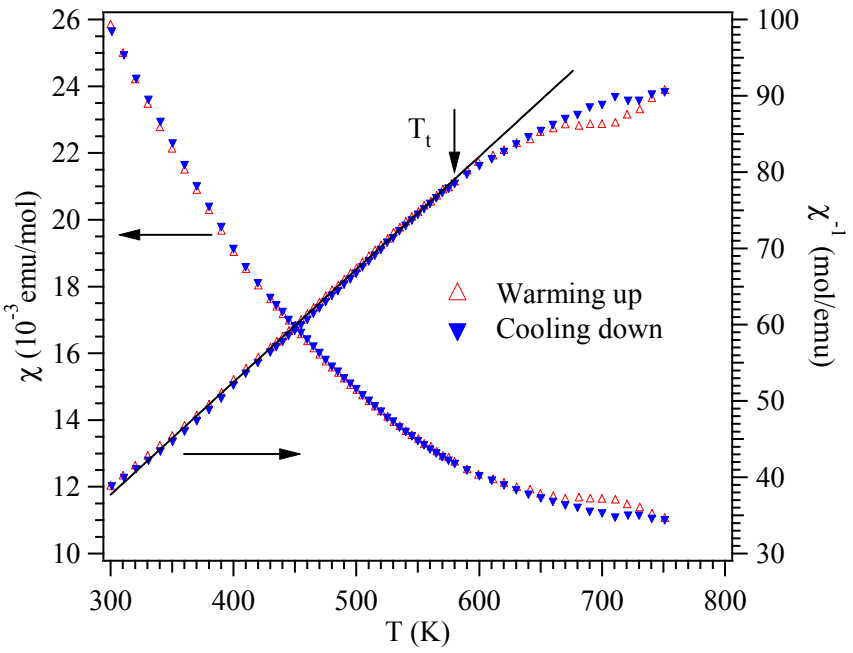

Fig. 3 (Color online) Temperature dependence of the magnetic susceptibility $\chi(T)$ and the inverse $\chi^{-1}(T)$ on heating up and cooling down between 300 and 750 K. The Curie-Weiss fitting curve is shown by the solid line.

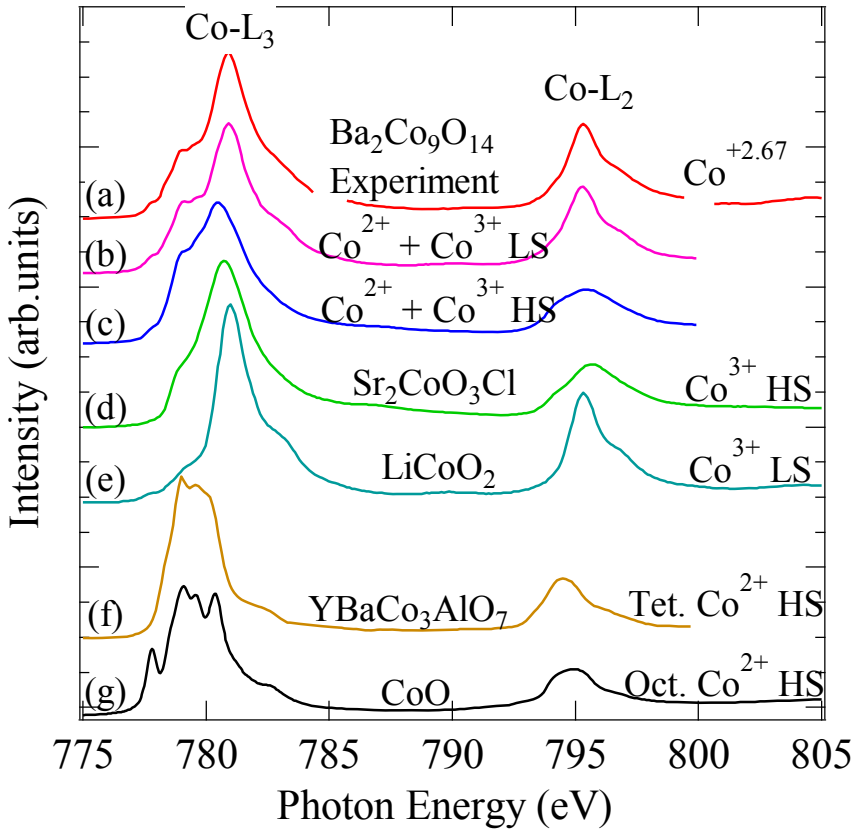

Fig. 4 (Color online) The Co-$L_{2,3}$ XAS spectra of (a) $Ba_2Co_9O_{14}$ and reference compounds, (b) and (c) are the simulated spectra (see the detail in the text), (d) Sr_2CoO_3Cl (Ref. 21), (e) $LiCoO_2$ (Ref. 24), (f) $YBaCo_3AlO_7$ (Ref. 25) and (g) CoO all taken at 300 K.

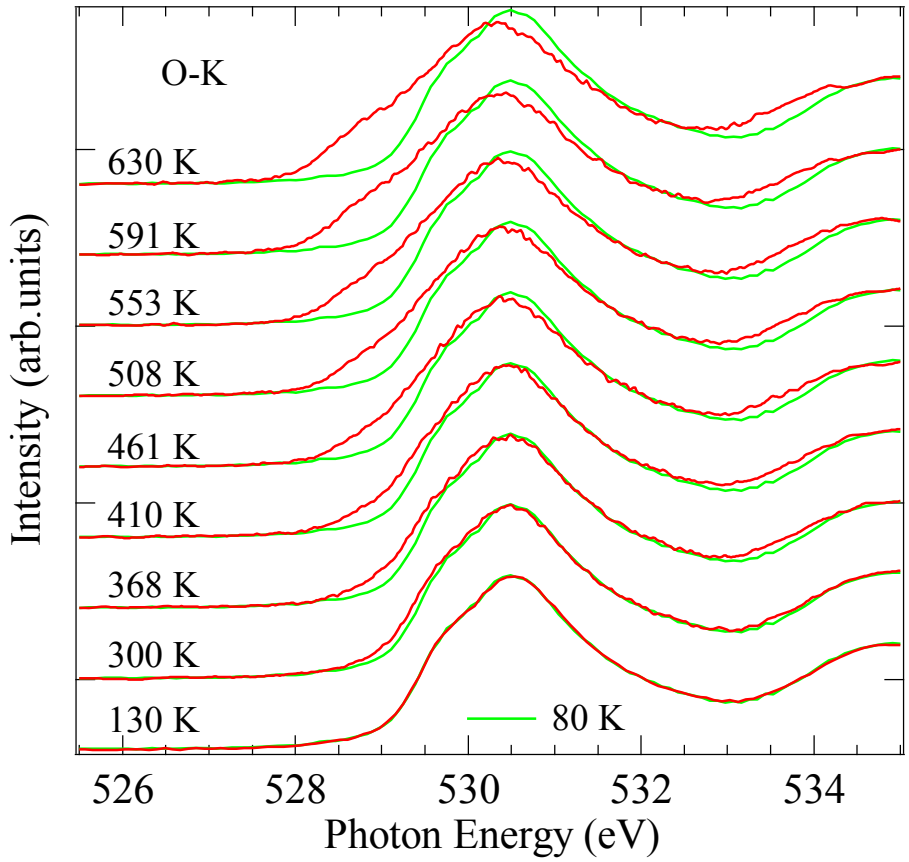

Fig. 5 (Color online) Temperature dependent O-K XAS spectra of $Ba_2Co_9O_{14}$. The green line presented at each temperature is taken at 80 K for comparison.

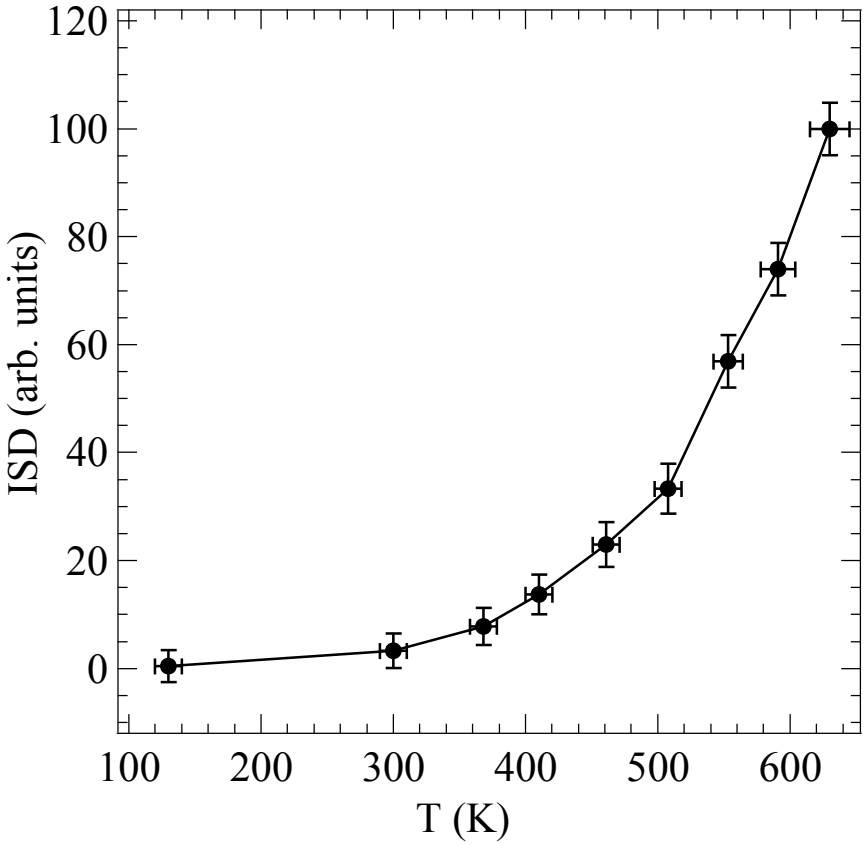

Fig. 6 Temperature dependence of ISD from the pre-edge peak in the O-K XAS spectra of $Ba_2Co_9O_{14}$.

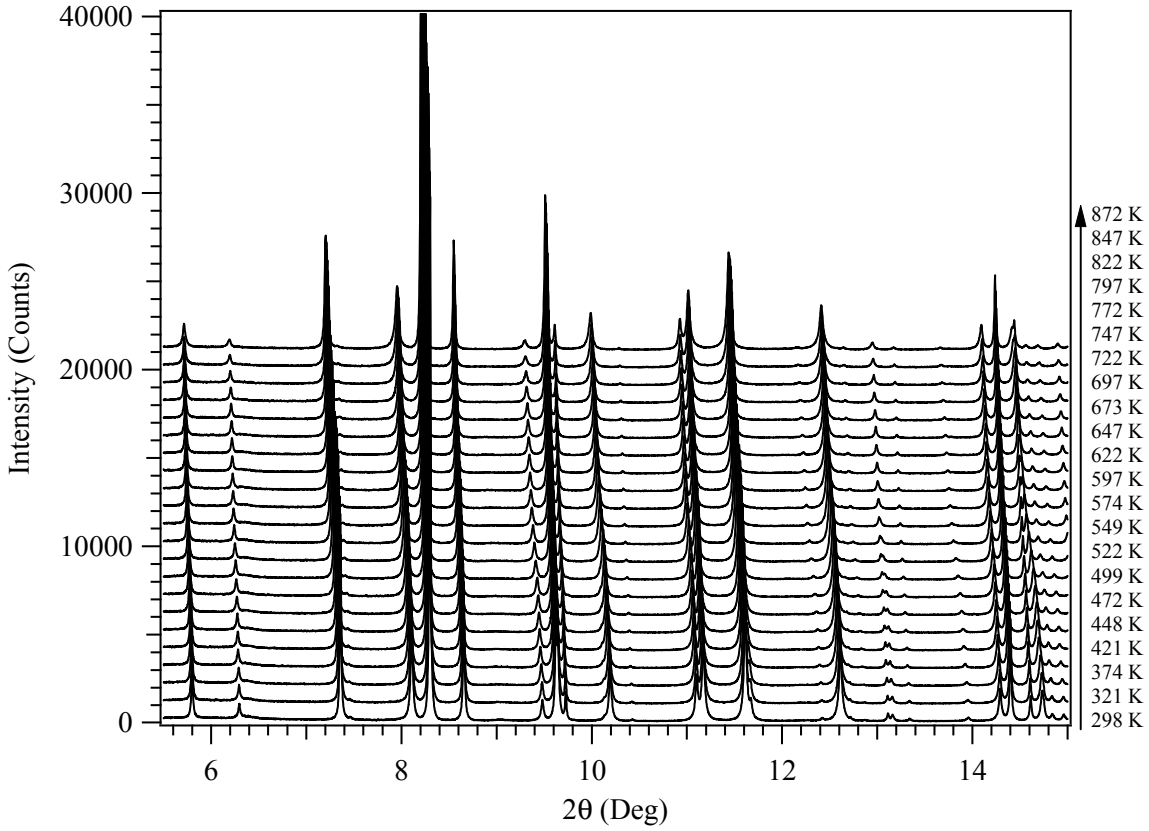

Fig. 7 High-resolution synchrotron x-ray diffraction patterns of $Ba_2Co_9O_{14}$ in the 2θ range 5 – 15° from 298 to 872 K.

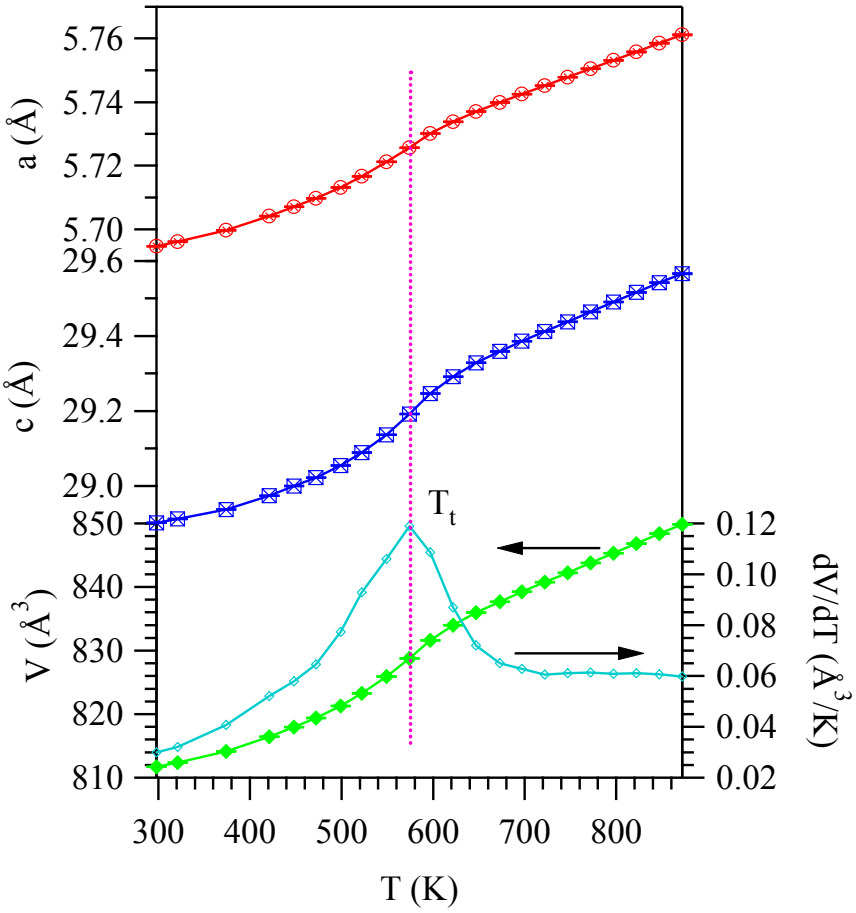

Fig. 8 (Color online) Temperature dependences of the unit-cell parameters *a*, *c*, *V* and the temperature derivative dV/dT.

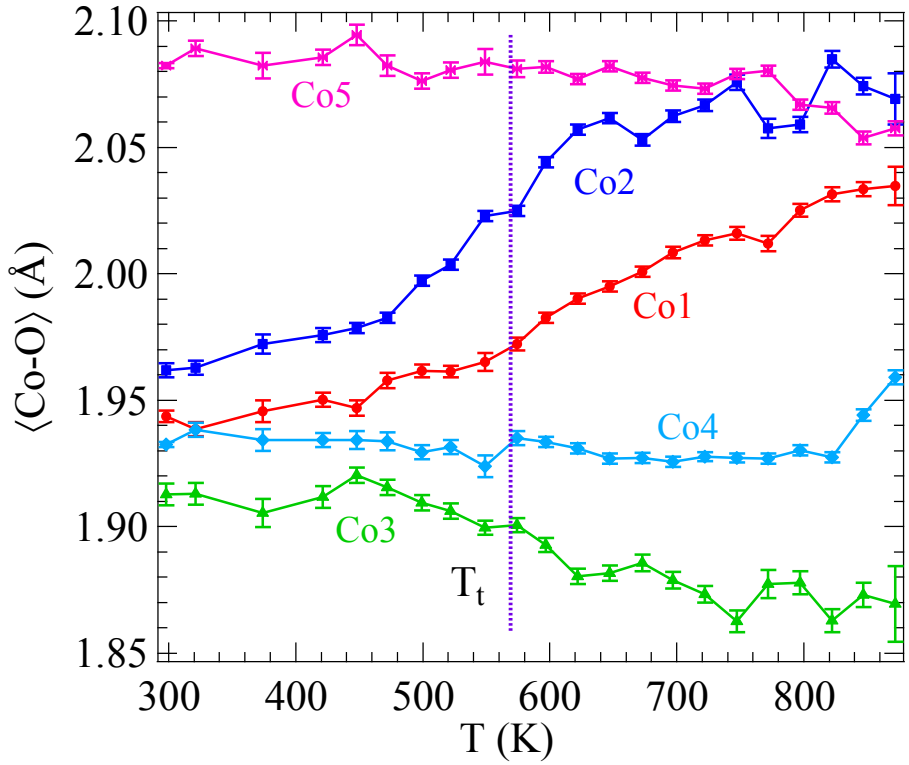

Fig. 9 (Color online) Temperature dependences of the average ⟨Co-O⟩ bond lengths for Co ions on different sites in $Ba_2Co_9O_{14}$.

References

[1] I. Terasaki, Y. Sasago, and K. Uchinokura, Phys. Rev. B **56**, R12685 (1997).

[2] K. Takada, H. Sakurai, E. Takayama-Muromachi, F. Izumi, R. A. Dilanian, and T. Sasaki, Nature (London) **422**, 53 (2003).

[3] A. C. Masset, C. Michel, A. Maignan, M. Hervieu, O. Toulemonde, F. Studer, and B. Raveau, Phys. Rev. B **62**, 166 (2000).

[4] D. Pelloquin, A. Maignan, S. Hebert, C. Martin, M. Hervieu, C. Michel, L. B. Wang, and B. Raveau, Chem. Mater. **14**, 3100 (2002).

[5] S. Sugano, Y. Tanabe, and H. Kaminura, *Multiplets of Transition-Metal Ions in Crystals*, (Academic, New York, 1970).

[6] J. B. Goodenough, in *Progress in Solid State Chemistry*, edited by H. Reiss (Pergamon, Oxford, 1971), Vol. **5**

[7] W. Koshibae, K. Tsutsui, and S. Maekawa, Phys. Rev. B **62**, 6869 (2000).

[8] A. Maignan, V. Caignaert, B. Raveau, D. Khomskii, and G. Sawatzky, Phys. Rev. Lett. **93**, 026401 (2004).

[9] Y. Diaz-Fernandez, L. Malavasi, and M. C. Mozzati, Phys. Rev. B **78**, 144405 (2008).

[10] C. Martin, A. Maignan, D. Pelloquin, N. Nguyen, and B. Raveau, Appl. Phys. Lett. **71**, 1421 (1997).

[11] L. Malavasi, Y. Diaz-Fernandez, M. C. Mozzati, and C. Ritter, Solid State Comm. **148**, 87 (2008).

[12] C. F. Chang, Z. Hu, Hua Wu, T. Burnus, N. Hollmann, M. Benomar, T. Lorenz, A. Tanaka, H.-J. Lin, H. H. Hsieh, C. T. Chen, and L. H. Tjeng, Phys. Rev. Lett. **102**, 116401 (2009).

[13] J. Sun, M. Yang, G. Li, T. Yang, F. Liao, Y. Wang, M. xiong, and J. Lin, Inorg. Chem **45**, 9151 (2006).

[14] G. Ehora, S. Daviero-Minaud, M. Colmont, G. André, and O. Mentré, Chem. Mater. **19**, 2180 (2007).

[15] J.-Q. Yan, J.-S. Zhou, and J. B. Goodenough, Phys. Rev. B **69**, 134409 (2004).

[16] T. Takami, S. Saiki, J.-G. Cheng, and J. B. Goodenough, J. Phys. Soc. Jpn. **79**, 114713 (2010).

[17] J. Wang, B. H. Toby, P. L. Lee, L. Ribaud, S. Antao, C. Kurtz, M. Ramanathan, R. B. von Dreele, and M. A. Beno, Rev. Sci. Instrum. **79**, 085105 (2008).

[18] J. Rodriguez-Carvajal, Physica B **192**, 55 (1993).

[19] J. Kanamori, Progress of Theoretical Physics **17**, 177 (1957).

[20] T. Burnus, Z. Hu, H. H. Hsieh, V. L. J. Joly, P. A. Joy, M. W. Haverkort, Hua Wu, A. Tanaka, H.-J. Lin, C. T. Chen, and L. H. Tjeng, Phys. Rev. B **77**, 125124 (2008).

[21] Z. Hu, H. Wu, M. W. Haverkort, H. H. Hsieh, H.-J. Lin, T. Lorenz, J. Baier, A. Reichl, I. Bonn, C. Felser, A. Tanaka, C. T. Chen, and L. H. Tjeng, Phys. Rev. Lett. **92**, 207402 (2004).

[22] M. W. Haverkort, Z. Hu, J. C. Cezar, T. Burnus, H. Hartmann, M. Reuther, C. Zobel, T. Lorenz, A. Tanaka, N. B. Brookes, H. H. Hsieh, H.-J. Lin, C. T. Chen, and L. H. Tjeng, Phys. Rev. Lett. **97**, 176405 (2006).

[23] T. Burnus, Z. Hu, M. W. Haverkort, J. C. Cezar, D. Flahaut, V. Hardy, A. Maignan, N. B. Brookes, A. Tanaka, H. H. Hsieh, H.-J. Lin, C. T. Chen, and L. H. Tjeng, Phys. Rev. B **74**, 245111 (2006).

[24] M. Abbate, S. M. Lala, L. A. Montoro, and J. M. Rosolen, Phys. Rev. B **70**, 235101 (2004).

[25] N. Hollmann, Z. Hu, M. Valldor, A. Maignan, A. Tanaka, H. H. Hsieh, H.-J. Lin, C. T. Chen, and L. H. Tjeng, Phys. Rev. B **80**, 085111 (2009).

[26] M Abbate, J. C. Fuggle, A. Fujimori, L. H. Tjeng, C. T. Chen, R. Potze, G. A. Sawatzky, H. Eisaki, and S. Uchida, Phys. Rev. B **47**, 16124 (1993).

[27] P. G. Radaelli and S.-W. Cheong, Phys. Rev. B **66**, 094408 (2002).

[28] Y. Ren, J.-Q. Yan, J.-S. Zhou, J. B. Goodenough, J. D. Jorgensen, S. Short, H. Kim, Th Proffen, S. Chang, and R. J. McQueeney, Phys. Rev. B. **84**, 214409 (2011).

[29] N. E. Brese and M. O'Keeffe, Acta. Cryst **47**, 192 (1991).

[30] I. D. Brown, Z. Kristallogr. **199**, 255 (1992).